Crystalline-like ordering of 8CB liquid crystals revealed by time-domain Brillouin scattering

Ievgeniia F Chaban, Christoph Klieber, Rémi Busselez, Keith A Nelson, Thomas Pezeril

Crystalline-like ordering of 8CB liquid crystals revealed by time-domain Brillouin scattering

Ievgeniia Chaban,[1,2,*] Christoph Klieber,[2,†] Rémi Busselez,[1] Keith A. Nelson,[2] and Thomas Pezeril[1,2,‡]

[1] *Institut Molécules et Matériaux du Mans, UMR CNRS 6283, Le Mans Université, 72085 Le Mans, France*
[2] *Department of Chemistry, Massachusetts Institute of Technology, Cambridge, MA 02139, USA*

(Dated: Wednesday 11th December, 2019)

We demonstrate that time-domain Brillouin scattering (TDBS), a technique based on an ultrafast pump-probe approach, is sensitive to phase transitions and apply it to the study of structural changes of 8CB liquid crystals at different temperatures across the isotropic, nematic, smectic and crystalline phases. We investigate the viscoelastic properties of 8CB squeezed in a narrow gap, from nanometer to submicrometer thickness range, and conclude on the long-range molecular structuring of the smectic phase. These TDBS results reveal that confinement effects favor structuring of the smectic phase into a crystalline-like phase that can be observed at extended distances far beyond the molecular dimensions.

I. INTRODUCTION

Liquid Crystal (LC) materials are well known from their unique phase transitions and thermotropic behavior that make them useful for a vast number of potential applications. Liquid crystalline materials exhibit a rich variety of polymorphism. The order of stability of the different phases varies on a scale of increasing temperature simply from the fact that a rise in temperature leads to a progressive destruction of molecular order. The more symmetric the mesophase, the closer in temperature it lies to the crystalline phase [1, 2].

One of the most rigorously studied LCs, 8CB, has drawn considerable attention in research regarding its prototypical thermotropic nature in phase transition studies. The properties of 8CB in bulk, or confined in nanosized pores, have been widely studied through light scattering, X-ray, dielectric, and calorimetric spectroscopic analyses by various authors [3–12]. Nonetheless, there is barely any information that connects the viscoelastic properties of 8CB across its structural phases with the confinement parameters over a wide range in liquid thicknesses. In general, the confinement conditions were only studied in ten's of nanometers pores [13, 14]. In order to fill this gap, we have performed TDBS measurements, which have been extensively used to investigate viscoelastic properties of materials in the GHz to THz frequency range [15], across different phases of 8CB bulk and confined in a submicrometer range of liquid thickness.

TDBS is an ultrafast pump-probe technique used to locally determine the light scattering frequency shift that manifests during the propagation of laser-excited ultrasound waves in a transparent or semi-transparent medium. Many examples have shown that TDBS is sensitive to diverse phenomena, including mechanical, optical or thermal inhomogeneities [16–23], non-linear acoustic waves [24, 25], or GHz transverse acoustic phonons in viscoelastic liquids [26–29].

In the present paper, we examine the different structural phases from TDBS data recorded at different temperatures or across a wide range of liquid thicknesses. We explore the situation of weakly confined 8CB, in the smectic phase as a bulk, in a thickness gap below few hundreds of nanometers. We presently report from our measurements crystalline-like molecular ordering of the weakly confined smectic phase.

II. APPARATUS AND TECHNIQUE

A. Sample

The temperature phase transitions of 4-N-octyl-CyanoBiphenyl ($C_{21}H_{26}N$), a liquid crystal with a rod-like molecule shape of about 20 Åin length, known under the name 8CB, are listed in Fig. 1(a) [1, 2]. At 313 K or higher, 8CB is in the isotropic phase for which the molecules are randomly oriented. When the isotropic liquid is cooled down below 313 K, the nematic phase emerges. The molecules tend to align along a particular director $\hat{n}$, while the molecules centers of mass are still isotropically distributed. With further cooling below 306.7 K, the nematic phase transforms to smectic A which forms liquid layers with a well-defined interlayer spacing [30, 31]. The smectic molecules exhibit some correlations in their positions in addition to the orientational ordering $\hat{n}$ normal to the layers. In the crystalline phase below 294 K, the molecular order is the highest. All nematic, smectic A and crystalline phases are optically anisotropic.

The samples in this study were prepared by squeezing 8CB between two substrates. One of these substrates, the so-called generation substrate, made of a flat n-dopped silicon substrate coated with a 40 nm Chromium film, acted as a photoacoustic transducer, as sketched in Fig. 1(b). The second substrate was an optically trans-

* ichaban@mit.edu
† Current address: Honeywell Process Solutions, Steinern Str. 19-21, 55252 Wiesbaden, Germany
‡ pezeril@mit.edu

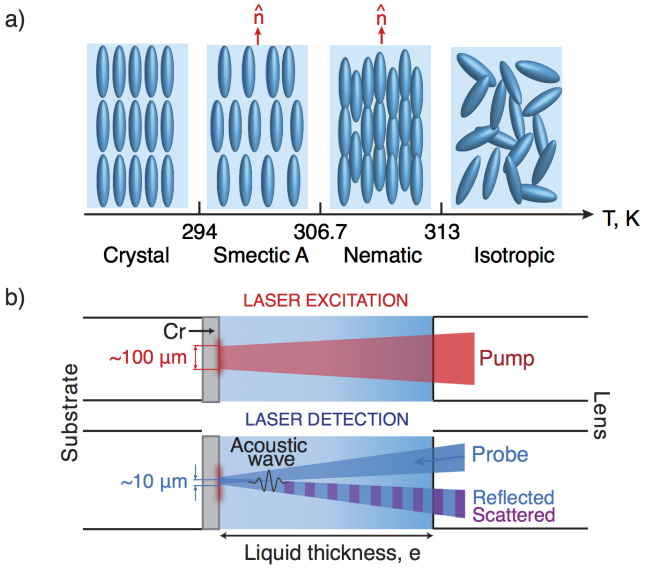

FIG. 1. (Color online) (a) Schematic representation of the molecule arrangement in the different phases of 8CB across the phase transition temperatures. (b) The liquid is squeezed between two substrates. One of them being a flat n-dopped Silicon substrate coated with a 40 nm Chromium film. The second is a plain glass plano-convex lens. The acoustic waves launched at the Cr film upon pump pulse irradiation are transmitted to the adjacent liquid layer where they are detected through TDBS by a delayed laser probe pulse.

parent glass plano-convex lens with a radius of curvature (ROC) of 386 mm. The generation substrate was glued on a nano-piezoelectric actuator in order to precisely control the liquid thickness gap between the substrate and the lens. The RMS roughness measured on both substrates is below one nanometer, which should not significantly alter any possible anchoring effect on the glass or the chromium surface [32].

B. Experimental methods

The optical experiment that we have built, is based on the TDBS technique, suitable for the investigation of viscoelastic liquids at GHz frequencies [26–29, 33, 34]. Measurements were made using an ultrafast optical pump-probe experimental setup as illustrated in Fig. 1(b). A femtosecond Ti-Sapphire Coherent RegA 9000 regenerative amplifier outputting femtosecond pulses of about 260 fs duration at a repetition rate of 260 kHz, tuned to a central wavelength of 790 nm has been used. The output beam was split into a pump and a probe beam. The pump was synchronously modulated at a subharmonic frequency of the laser repetition rate by an acousto-optic modulator (AOM). After the AOM, the pump beam passed through a motorized delay stage which allowed a continuous modification of the time difference between the pump and probe pulses of different optical paths. At the sample, the pump beam was focused on the surface of a Chromium film with a Gaussian spatial beam profile of FWHM ∼100 μm. The lowest possible pump fluence of only 0.5 mJ·cm^{-2} was chosen to avoid cumulative heating of the liquid. The corresponding steady state temperature rise, calculated from [23], was of 3 K only. The probe beam, of significantly weaker intensity, was frequency doubled to 395 nm wavelength through optical second harmonic generation. The circularly polarized probe was tightly focused at normal incidence on the sample surface with a spot size of about 10 μm FWHM, and spatially overlapped with the pump spot to monitor the acoustic waves propagation in the liquid sample. As sketched in Fig. 1(b), part of the pump optical energy got absorbed over the optical skin depth of the chromium film and converted into heat, which resulted in a lattice temperature rise leading to a thermal stress that launched an acoustic wavepacket. This laser excited acoustic wavepacket got then partially transmitted across the metal/liquid interface into the adjacent transparent liquid. The acoustic propagation of the wavepacket through the liquid film of thickness e was monitored by TDBS. The probe beam reflected by the transducer film and scattered by the propagating acoustic wavepacket was directed to a photodiode connected to a lock-in amplifier synchronized to the pump modulation frequency to measure its transient differential reflectivity ΔR(t) as a function of time delay between pump and probe beams. The propagation of the acoustic wavepacket in a transparent liquid medium leads to the occurrence of TDBS oscillations on the transient reflectivity signal, as seen on the data displayed on Fig. 2. The TDBS scattering oscillations can be described by the functional form

$$\triangle R = A_0 \exp(-\Gamma t) \cos(2\pi \nu_{_B} t + \phi), \qquad (1)$$

where A_0 is the initial amplitude, Γ is the acoustic attenuation rate and ϕ an arbitrary phase. The Brillouin frequency $\nu_{_B}$ is determined by

$$\nu_{_B} = \frac{2\, n\, c_l}{\lambda} \cos\theta, \qquad (2)$$

where θ is the back-scattering angle, n the index of refraction, c_l the acoustic velocity in the sample medium, and λ the probe wavelength.

III. RESULTS

A. 8 CB phase transitions

We have performed TDBS temperature dependent measurements of bulk 8CB in order to monitor the changes in the structural properties of each phase under our specific optical configurations. The liquid sample cell was placed in a temperature controlled cryostat, that ensures a temperature stability better than 0.1° C. The measurements were performed at a very slow temperature change (∼ 1°C/min) and the sample was held

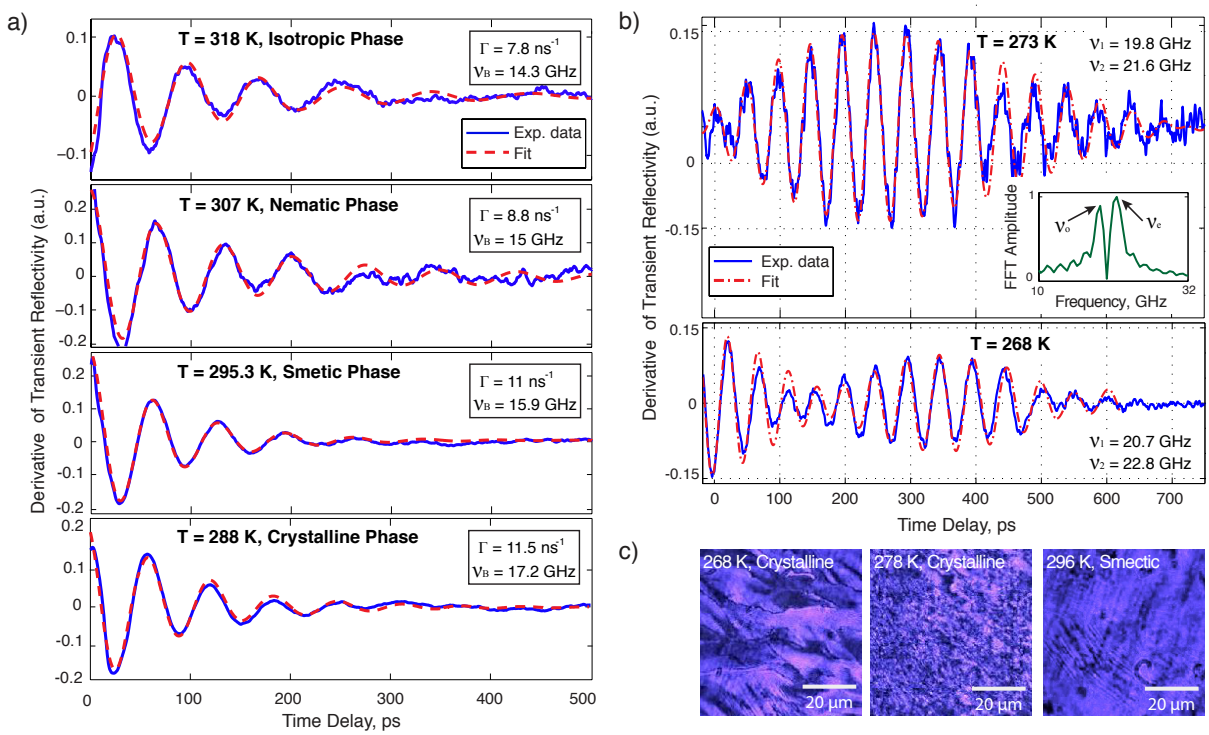

FIG. 2. (Color online) (a) Representative TDBS signals recorded with 8CB at different specified temperatures. While cooling down the LC from 318 K to 288 K, the liquid undergoes three phase transitions. The fit parameters for different temperatures show that the Brillouin scattering frequency ν_B and the damping rate Γ varies as a function of temperature. (b) Recorded TDBS signals at temperatures well below the smectic to crystalline phase transition. We observe the coexistence of two Brillouin modes, as revealed by the FFT in inset of the top plot. (c) Microscope images of the sample obtained with a crossed polarizer at different temperatures. The TDBS measurements were performed with circularly polarized light at normal incidence.

at constant temperature for a long time for liquid homogenization and temperature stabilization. At the sample location where we have performed these TDBS measurements, the corresponding liquid thickness was in the range of tens of microns. Figure 2(a) shows several TDBS data obtained for bulk 8CB at selected temperatures across the LCs phase transitions. The experimental data were fitted using Eq. (1). The uncertainties of the fit are in the range of ± 0.1 GHz for the frequency determination and ± 0.2 ns^{-1} for the damping rate estimate. The fit parameter ν_B for different temperatures shows that the Brillouin scattering frequency increases while cooling the LC, which is consistent with the fact that the liquid becomes denser and stiffer when the phases approach the most ordered and compact crystalline phase. Despite of the fact that 8CB exhibits high optical birefringence, we could only detect one single Brillouin scattering frequency for smectic and crystalline phases. This is most probably not related to homeotropic anchoring but rather a signature of the randomized director orientation of the domains in the probed volume. This is consistent with the fact that the birefringence appears on the TDBS data only in wide LCs domains, as indicated on Fig.2(b) and (c). Note that the general trend of an increase of the attenuation rate for a temperature decrease in the range 318 K - 288 K, see Table 1, is an apparent counterintuitive temperature evolution. The attenuation rate is commonly known to be smaller for well-ordered crystals than for disordered liquids. As highlighted in Fig. 2(c), the liquid texture evolution with temperature should be accounted to explain this unusual behavior.

B. Crystalline texture of 8CB

Experiments at temperatures well below the crystalline phase transition were performed in a similar manner to primarily investigate the 8CB crystalline texture evolution with temperature. As highlighted on the microscope

Temperature	ν_B, GHz	Γ, ns^{-1}	c_l, m/s	n_{eff} [36]
318 K (Is)	14.3	7.8	1810	1.56
307 K (Nm)	15	8.8	1860	1.59
295.3 K (Sm)	15.9	11	1960	1.6
288 K (Cr)	17.2	11.5	2120	1.6
273 K (Cr)	19.8, 21.6	2.5	2560	1.51, 1.68
268 K (Cr)	20.7, 22.8	2.5	2690	1.51, 1.68

TABLE I. Viscoelastic properties of bulk 8CB across different thermotropic phases (Is, Nm, Sm, Cr), extracted from our TDBS measurements.

images shown in Fig. 2(c), a significant texture modification occurs in the crystalline phase. When the crystalline sample is cooled further and further, the crystallites grow more and more in size and eventually exceed the probe spot dimension. As can be observed from the signal spectrum in Fig. 2(b) inset, we experimentally observe the coexistence of two Brillouin modes at temperatures well below the crystalline temperature transition, that indicates that TDBS occurs in single, or just a few, domains. As in [35], in case of single domains, the birefringence is not hidden anymore by the averaging process over multiple grains orientations across the probe spot area. For a circularly polarized probe, the transient optical reflectivity exhibits some beatings in the time domain that correspond to the presence of two Brillouin modes, an ordinary and an extraordinary, with slightly different frequencies. This frequency beating is clearly visible in each plot of Fig. 2(b), that shows the experimental data and the theoretical fit of Brillouin scattering oscillations in bulk 8CB in the crystalline phase. The Brillouin frequencies ratio $\nu_{B,e}/\nu_{B,o} \approx 1.09$ for all range of temperatures measured experimentally on Fig. 2(b) are close to the ratio of $n_e/n_o = 1.13$ [36], which infers that the effective index matches the extraordinary index n_e. This observation is consistent with a birefringence effect revealed by the TDBS data and discloses any possible effect related to the anisotropic acoustic propagation in the crystallites. The Brillouin scattering frequencies increase progressively when the temperature decreases, which is consistent with the general trend that the crystalline phase becomes stiffer when the texture resembles more and more a well-defined bulk crystal. The determined values of the Brillouin scattering frequencies at both temperatures allow to calculate the sound velocity of bulk 8CB in the crystalline phase using Eq. (2) and the measured refractive indices in [36]. The values derived from the measurements at T = 273 K or T = 268 K are listed in Table 1. It should be noted that at such low temperatures below the crystallization temperature, the observed acoustic damping rate $\Gamma = 2.5$ ns^{-1} is significantly lower than for the data shown in Fig. 2(a) obtained at higher temperatures. The fact that the attenuation rate drops in the crystalline phase with wide LCs domains, in the temperature range 273 K - 268 K, evidence the predominant influence of texture in the measured attenuation rate. The coexistence of multiple domains in the ordered phases leads to a significant acoustic attenuation due to the propagation of the acoustic waves throughout multiple structural domains of different orientations. These results confirm that the random texture dominates the acoustic attenuation on the data shown in Fig. 2(a).

C. 8CB under submicrometer confinement

In addition to temperature dependent measurements performed on bulk 8CB, we have performed TDBS measurements on 8CB liquid films of variable thicknesses in the submicron range, at a temperature of 295 K where bulk 8CB is in the smectic phase. The liquid cell that we have employed in order to achieve a tunable liquid thickness topography is based on a lens/flat substrate configuration, as described in [26, 27, 33]. The liquid was squeezed between a lens of well-defined ROC and the generation substrate holding the optical transducer film. The ROC was chosen as a compromise such that the liquid variation across the probe spot size can be neglected and such that the liquid can easily flow by pushing both sides of the sample until the lens gets in direct contact with the substrate. The liquid thickness e variation for a distance r away from the direct contact point where there is no liquid at all, follow this classical relationship of a curved-flat topography,

$$e = \frac{r^2}{2 \times \mathrm{ROC}}. \tag{3}$$

In practice, we have recorded TDBS data for many lateral positions away from the contact point. Each lateral position corresponds to a well defined liquid thickness that follows equation Eq. (3). 2D results obtained from 70 lateral measurements are presented in Fig. 3 (a). There is a wealth of information that can be extracted from such a data set. The central zone where $r \sim 0$ corresponds to a liquid thickness well below 10 nm and we observe high-frequency signal oscillations due to Brillouin scattering in the lens at $\approx$ 46 GHz. Away from the center, as the liquid thickness increases, these oscillations get time delayed and attenuated. As in [26, 27, 33], since the liquid topography is well defined, the values for the speed of sound and attenuation rate at 46 GHz in 8CB can be derived from the spectral phase evolution shown in Fig. 3 (b) and spectral amplitude evolution in Fig. 3 (c). The fitted value for the sound velocity at 46 GHz is $c_l = 2600 \pm 50$ m·s^{-1} and the attenuation rate is $\Gamma = 29.5 \pm 1$ ns^{-1}. As a comparison, the sound velocity of the smectic phase at 295 K measured through Brillouin scattering at 8 GHz in [37] is 1800 m·s^{-1}. The measured speed of sound at 46 GHz clearly matches the crystalline phase speed of sound extracted at 20 GHz from our TDBS measurements in bulk 8CB, see Table 1. If we neglect the acoustic dispersion of the speed of sound in this frequency range, it clearly indicates an interface structuring of the 8CB smectic phase at room temperature. The high value of the attenuation rate implies that the LC is far from being a well defined single domain structure and that the acoustic attenuation is mainly caused by scattering throughout multiple domains.

Away from the center, in a thickness range higher than 300 nm on Fig. 3(a), low-frequency signal oscillations at 15.7 GHz with a corresponding damping rate of $\Gamma = 11$ ns^{-1} appear. Both values clearly match the Brillouin frequency and damping rate of the smectic phase that we have measured in bulk 8CB, see Table 1. We can conclude that somewhere below 300 nm in thickness, a crystalline-like structure with similarities with the crys-

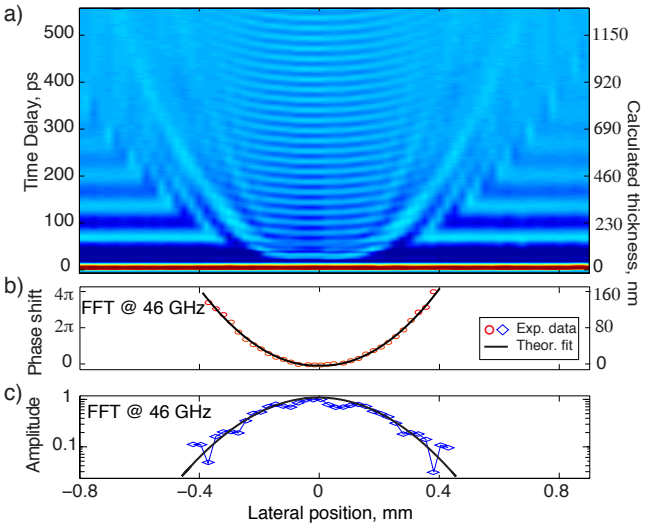

FIG. 3. (Color online) (a) Computed image of TDBS data measured at many different lateral positions r. The color bar is arbitrarily chosen to best highlight the TDBS amplitude of the data obtained from 8CB at 295 K. The high-frequency oscillations at 46 GHz that correspond to Brillouin scattering in the lens can be seen at the vicinity of the contact area for which $r \sim 0$. The low-frequency oscillations at 15.7 GHz, seen further away from the contact area, correspond to Brillouin scattering in bulk smectic 8CB. (b) Phase shift and (c) normalized amplitude of the 46 GHz Brillouin oscillations versus lateral position.

talline phase of bulk 8CB is revealed by these TDBS measurements.

IV. SUMMARY

In the present paper, we have studied the temperature evolution of TDBS data across the different LCs phases and emphasized the link between LC texture and acoustic attenuation rate. We have conducted experiments in narrow liquid gaps to investigate structural transitions in weakly confined liquids. Unlike conventional Brillouin light scattering, which is limited by the optical wavelength and cannot study samples below a few microns in thicknesses, our sophisticated TDBS technique permits measurements of Brillouin signals in submicron liquid gaps with a resolution in the ten's of nanometers range. Our results presently discussed highlight the existence of a well-structured phase, intermediate from the smectic and crystalline phases, which is caused by positional ordering of the 8CB molecules induced by submicrometric confinement. Our technique of TDBS performed under a wide range of liquid thicknesses, from nanometer to submicrometer, can appropriately determine and follow the structural organization of liquids.

Temperature dependent measurements are under way to determine the thermodynamic character of this structural ordering. Further improvements of the technique could open new perspectives for the investigation of liquid confinement based on GHz ultrasonic probing with molecular resolution, complementarily to the surface force apparatus technique that can reveal out-of-equilibrium liquid confinement [38–40].

Overall, our results go far beyond the topic of liquid crystals and illustrate the usefulness of TDBS that can be performed in all sorts of nano-liquids to outcome unprecedented new information on the mechanical properties of soft materials at the nano-scale.

Acknowledgements

The authors acknowledge financial support from Agence Nationale de la Recherche under Grant Plusdil No. ANR-12-BS09-0031. The authors would like to thank Lionel Guilmeau, Mathieu Edely and Sébastien Nogarotto for technical support and expertise.

[1] S. Singh, D. A. Dunmur, Liquid Crystals: Fundamentals, World Scientific Co Pte. Ltd., New Jersey, London, Singapore, Hong Kong, (2002).
[2] S. Singh, Phys. Reports **324**, 107 (2000).
[3] J. Thoen, H. Marynissen, W. Van Dael, Phys. Rev. A **26**, 2886 (1982).
[4] G. Iannacchione, D. Finotello, Phys. Rev. Lett. **69**, 2094 (1992).
[5] T. Stoebe, R. Geer, C. C. Huang, J. W. Goodby, Phys. Rev. Lett. **69**, 2090 (1992).
[6] M. Marinelli, F. Mercuri, S. Foglietta, U. Zammit, F. Scudieri, Phys. Rev. E **54**, 1604 (1996).
[7] C. Glorieux, P. De Schrijver, P. Johnson, O. Balus, C., Serban, C. Huang, J. Thoen, Mol Cryst Liq Cryst Sci Tech Sec A: Mol Cryst Liq Cryst **329**, 663 (1990).
[8] C. Fehr, Ph. Dieudonne, J. Primera, T. Woignier, J.-L. Sauvajol, E. Anglaret, Eur. Phys. J. E **12**, s01 004 (2003).
[9] Physical Properties of Liquid Crystals, ed. by D. Demus, J. Goodby, G. W. Gray, H.-W. Spiess, V. Vill, - Weinheim; New York; Chichester; Brisbane; Singapore; Toronto: Wiley - VCH, 1999.
[10] A. Zidanšek, G. Lahajnar, S. Kralj, Appl. Magn. Reson. **27**, 311 (2004).
[11] D. Sharma, J. C. MacDonald, G. S. Iannacchionne, J. Phys. Chem. **110**, 16679 (2006).
[12] O. Oltutu, F. Cakirtas, N. Yorulmaz, S. Yilmaz, Phase Transitions **89**, 242 (2016).
[13] T. Bellini, L. Radzihovsky, J. Toner, N. Clark, Science **294**, 1074 (2001).
[14] R. Guegan, D. Morineau, R. Lefort, W. Beziel, M. Guendouz, L. Noirez, A. Henschel, P. Huber, Eur. Phys. J. E

26, 261 (2008).
[15] H. N. Lin, R. J. Stoner, H. J. Maris, J. Tauc, J. Appl. Phys. **69**, 3816 (1991).
[16] C. Mechri, P. Ruello, J.-M. Breteau, M. Baklanov, P. Verdonck, V. Gusev, Appl. Phys. Lett. **95**, 091907 (2009).
[17] A. Steigerwald, Y. Xu, J. Qi, J. Gregory, X. Liu, J.K. Furdyna, K. Varga, A.B. Hmelo, G. Lüpke, L.C. Feldman, N. Tolk, Appl. Phys. Lett. **94**, 111910 (2009).
[18] A. M. Lomonosov, A. Ayouch, P. Ruello, G. Vaudel, M. R. Baklanov, P. Verdonck, L. Zhao, V. E. Gusev, ACS Nano **6**, 1410 (2012).
[19] S. Nikitin, N. Chigarev, V. Tournat, A. Bulou, D. Gasteau, B. Castagnede, A. Zerr, V. Gusev, Scientific reports **5**, 9352 (2015).
[20] T. Dehoux, M. Ghanem, O. Zouani, M. Ducousso, N. Chigarev, C. Rossignol, N. Tsapis, M.-C. Durrieu, B. Audoin, Ultrasonics **56**, 160 (2015).
[21] S. Danworaphong, M. Tomoda, Y. Matsumoto, O Matsuda, T. Ohashi, H. Watanabe, M. Nagayama, K. Gohara, P. H. Otsuka, O. B. Wright, Appl. Phys. Lett. **106**, 163701 (2015).
[22] F. Pérez-Cota, R. J. Smith, E. Moradi, L. Marques, K. F. Webb, M. Clark, Appl. Opt. **54**, 8388 (2015).
[23] I. Chaban, H. D. Shin, C. Klieber, R. Busselez, V. Gusev, K. Nelson, T. Pezeril, Rev. of Sci. Instrum. 88, 074904 (2017)
[24] C. Klieber, T. Pezeril, V. Gusev, K. A. Nelson, Phys. Rev. Lett. **114**, 065701 (2015).
[25] A. Bojahr, M. Herzog, D. Schick, I. Vrejoiu, and M. Bargheer, Phys. Rev. B **86**, 144306 (2012).
[26] T. Pezeril, C. Klieber, S. Andrieu, K. A. Nelson, Phys. Rev. Lett. **102**, 107402 (2009).
[27] C. Klieber, T. Pezeril, S. Andrieu, K. A. Nelson, J. Appl. Phys. **112**, 013502 (2012).
[28] C. Klieber, T. Hecksher, T. Pezeril, D. H. Torchinsky, J. C. Dyre, and K. A. Nelson, J. Chem. Phys. **138**,12A544 (2013).
[29] T. Pezeril, Opt. & Laser Tech. **83**, 177 (2016).
[30] R. L. McMillan, Phys. Rev. A **7**, 1673 (1973).
[31] L. Wu, M. Young, Y. Shao, C. Garland, R. Birgencau, Phys. Rev. Lett. **72**, 376 (1994).
[32] O. Roscioni, L. Muccioli, R. Della Valle, A. Pizzirusso, M. Ricci, C. Zannoni, Langmuir **29**, 8950 (2013).
[33] C. Klieber, Ph.D. Thesis, http://hdl.handle.net/1721.1/57801, MIT (2010).
[34] L. Shelton, F. Yang, W. K. Ford, and H. J. Maris, Phys. Stat. Sol. (b) **242**, 1379 (2005).
[35] M. Lejman, I. C. Infante, G. Vaudel, I. Chaban, M. Edely, P. Gemeiner, G. Nataf, J. Kreiser, V. Gusev, B. Dkhil, P. Ruello, Nat. Commun. **7**, 12345 (2016).
[36] R. Horn, J. Phys. **39**, 105 (1978).
[37] G. Bradberry, J. Vaughan, J. Phys. C: Solid state Physics **9**, 3905 (1976).
[38] S. Granick, Science **253**, 1374 (1991).
[39] J. Klein, E. Kumacheva, Science **269**, 816 (1995).
[40] M. Heuberger, M. Zach, N. D. Spencer, Science **292**, 905 (2001).